

# Unveiling spatial and temporal heterogeneity of a tropical forest canopy using high-resolution NIRv, FCVI, and NIRvrad from UAS observations

Trina Merrick<sup>1</sup>, Stephanie Pau<sup>2</sup>, Matteo Detto<sup>3,4</sup>, Eben N. Broadbent<sup>5</sup>, Stephanie. A. Bohlman<sup>3,6</sup>, Christopher J. Still<sup>7</sup>, Angelica M. Almeyda Zambrano<sup>8</sup>

<sup>1</sup> Naval Research Laboratory, Remote Sensing Division, 4555 Overlook Ave. SW, Washington, DC, 20375, USA

<sup>2</sup> Department of Geography, Florida State University, 113 Collegiate Loop, Tallahassee, Florida 32306, USA

<sup>3</sup> Smithsonian Tropical Research Institute, Apartado 0843-03092, Balboa, Ancon, Panama

<sup>4</sup> Department of Ecology and Evolutionary Biology, Princeton University, Princeton, New Jersey 08544 USA

<sup>5</sup> Spatial Ecology and Conservation Lab, School of Forest, Fisheries and Geomatics Sciences, University of Florida, Gainesville, FL, 32608 USA

<sup>6</sup> School of Forest, Fisheries and Geomatics Sciences, University of Florida, Gainesville, FL, 32608 USA

<sup>7</sup> Department of Forest Ecosystems and Society, Oregon State University, Corvallis, Oregon 97331 USA

<sup>8</sup> Spatial Ecology and Conservation Lab, Center for Latin American Studies, University of Florida, Gainesville, Florida 32608 USA

\*<sup>2</sup> Primary author former affiliation

*Correspondence to:* Trina Merrick (trina.merrick@nrl.navy.mil)

**Abstract.** Recently, remotely-sensed measurements of the near-infrared reflectance (NIRv) of vegetation, the fluorescence correction vegetation index (FCVI), and radiance (NIRvrad) of vegetation, have emerged as indicators of vegetation structure and function with potential to enhance or improve upon commonly used indicators, such as the normalized difference vegetation index (NDVI) and the enhanced vegetation index (EVI). The applicability of these remotely sensed indices to tropical forests, key ecosystems for global carbon cycling and biodiversity, have been limited. In particular, fine-scale spatial and temporal heterogeneity of structure and physiology may contribute to variation in these indices and the properties that are presumed to be tracked by them, such as gross primary productivity (GPP) and absorbed photosynthetically active radiation (APAR). In this study, fine-scale (approx. 15cm) tropical forest heterogeneity represented by NIRv, FCVI, and NIRvrad, and by lidar-derived height is investigated and compared to NIRv and EVI using unoccupied aerial system (UAS)-based hyperspectral and lidar sensors. By exploiting near-infrared signals, NIRv, FCVI, and NIRvrad captured the greatest spatiotemporal variability, followed by the enhanced vegetation index (EVI), then the normalized difference vegetation index (NDVI). Wavelet analyses showed the dominant spatial scale of variability of all indicators was driven by tree clusters and larger-than-tree-crown size gaps rather than individual tree crowns. NIRv, FCVI, NIRvrad, and EVI captured variability at smaller spatial scales (~50 m) than NDVI (~90 m) and lidar-based surface model (~70 m). We show that spatial and temporal patterns of NIRv and FCVI were virtually identical for a dense green canopy, confirming predictions in earlier studies. Furthermore, we show that NIRvrad, which does not require separate irradiance measurements, correlated more strongly with GPP and PAR than did other indicators. NIRv, FCVI, and NIRvrad, which are related to canopy structure and the radiation regime of vegetation canopies, are promising tools to improve understanding of tropical forest canopy structure and function.

## 42 1 Introduction

43 Important spatial and temporal heterogeneity in structurally complex and species-rich tropical forests is not well  
44 characterized. Many factors contributing to this heterogeneity, including varying microclimate, light conditions,  
45 topography, crown structure, and patterns of tree mortality and regeneration, can produce high variability in carbon  
46 fluxes, ultimately affecting coarse-scale gross primary production (GPP) measurements in forests (e.g., Xu et al., 2015;  
47 Guan et al., 2015; Morton et al., 2014; Bohlman and Pacala, 2012; Laurance et al., 2012; Clark et al., 2008; Huete et  
48 al., 2008). Improving knowledge of tropical forest dynamics at multiple scales is crucial to monitoring and predicting  
49 resilience of tropical ecosystems and productivity under climate change (Liu et al., 2021; Clark et al., 2017; Laurance  
50 et al., 2012; Malhi, 2012; Wright, 2010; Saatchi et al., 2010; Lewis et al., 2009). Remote sensing (RS) measurements  
51 have been employed to uncover vegetation patterns of structure and productivity from local to global scales, often  
52 with a focus on filling gaps in knowledge regarding variation and uncertainties in GPP estimates (e.g., Jung et al.,  
53 2011; Glenn et al., 2008; Huete et al., 2002; Ryu et al., 2018; Yang et al., 2017; Jiang et al., 2008; Zhao et al., 2010;  
54 Heinsch et al., 2006; Running et al., 2004; Turner et al., 2003). Yet, the spatial mismatch between satellite data (e.g.,  
55 30 m to 1 km pixel resolution), which provides observations across large extents at repeat intervals, and site-specific  
56 plot level data (e.g., 0.1 – 1 hectare), is in part responsible for the uncertainties in GPP estimates. Yet, there is a spatial  
57 mismatch between satellite data (e.g., 30 m to 1 km pixel resolution), which provides observations across large extents  
58 at repeat intervals, and plot level data, is in part responsible for the uncertainties in GPP estimates (Gelybó et al.,  
59 2013; Zhang et al., 2020). A way to solve this problem is to acquire high spatial and temporal resolution data that can  
60 capture fine-grained heterogeneity of tropical forests (Clark et al., 2017; Mitchard, 2018; Saatchi et al., 2011; Lewis  
61 et al., 2009). Unoccupied aerial systems (UAS) with hyperspectral imaging sensors offer an opportunity to collect  
62 tropical forest canopy data at high spatial resolution and which could address unknowns related to the high  
63 heterogeneity of tropical forests.

64 Traditional reflectance-based indices (RI) using RS data, such as the normalized difference vegetation index  
65 (NDVI) and enhanced vegetation index (EVI), are known to capture structural changes that are coincident with  
66 changes in GPP. RIs have provided optical methods using RS to track GPP via the light use efficiency (LUE) model  
67 (J.L.Monteith, 1977; Yuan et al., 2014; B. E. Medlyn, 1998). In the most commonly used formulation of the LUE  
68 model for RS, GPP is

$$69 \quad GPP = APAR \times \varepsilon \quad (1)$$

70 where APAR is the absorbed photosynthetically active radiation and ( $\varepsilon$ ) is the efficiency with which the target  
71 vegetation converts the radiation to carbon (Gamon, 2015; Yuan et al., 2014; Running et al., 2004). APAR is derived  
72 from

$$73 \quad APAR = PAR \times fPAR \quad (2)$$

74 where PAR is the incoming photosynthetically active radiation and fPAR is the fraction of absorbed PAR. RIs  
75 commonly used in the LUE model of GPP as well as direct proxies for GPP are NDVI and EVI, because of a strong  
76 relationship to fPAR (Springer et al., 2017; Morton et al., 2015; Gamon et al., 2015; Porcar-Castell et al., 2014; Glenn  
et al., 2008; Gao et al., 2007; Huete et al., 2002; Zarco-Tejada et al., 2013). NDVI and EVI are typically used as

77 proxies on seasonal timescales. When used to examine changes on shorter timescales, they have been multiplied by  
78 photosynthetically active radiation (PAR) to account for changes in radiation (incoming, absorbed, and scattered)  
79 which better align with GPP changes (Springer et al., 2017; Yuan et al., 2014). However, RIs alone have often not  
80 shown enough sensitivity to capture more fine-scale or rapid changes in vegetation, such as those in tropical forests,  
81 and questions linger about the ability to track green-up with RIs in evergreen regions (Liu et al., 2021; Yang et al.,  
82 2018a; Lee et al., 2013; Xu et al., 2015; Morton et al., 2014; Samanta et al., 2010; Sims et al., 2008).

83 Recently, three emerging vegetation indicators have been shown to track with GPP more closely than traditional  
84 RIs. These indicators are the near-infrared reflectance of vegetation (NIRv) (Badgley et al., 2017), the fluorescence  
85 correction vegetation index (FCVI) (Yang et al., 2020) and the near-infrared radiance of vegetation (NIRvrad) (Wu et  
86 al., 2020). Because they exploit additional information from the NIR region of the spectrum, NIRv, FCVI, and  
87 NIRvrad do not saturate in dense canopies or suffer the same level of contamination from senesced vegetation and  
88 soils as traditional RIs (Baldocchi et al., 2020; Badgley et al., 2017). Additionally, these indicators require only  
89 moderate spectral resolution data and are similarly straightforward to measure and calculate as RIs, making them  
90 accessible in a broad range of studies. Therefore, NIRv, FCVI, and NIRvrad could be employed as valuable indicators  
91 of canopy structure and function (Badgley et al., 2019; Badgley et al., 2017; Dechant et al., 2020).

92 NIRv is the product of NDVI and the total near-infrared scene reflectance (NIR). NIRv from moderate  
93 spectral resolution satellite imagery and field spectrometers has been shown to empirically track both measured and  
94 modelled GPP globally, although with highest uncertainties in the tropics. The NIRv~GPP relationship holds at  
95 monthly to seasonal timescales presumably due to co-incident changes in canopy phenology, light capture and  
96 scattering, and GPP (Badgley et al., 2019; Badgley et al., 2017; Dechant et al., 2020). FCVI, derived from radiative  
97 transfer theory rather than an empirical relationship, is calculated from RS data by subtracting the reflectance in the  
98 NIR from the reflectance in the visible range (Yang et al., 2020). Yang et al. (2020) demonstrated that FCVI tracked  
99 GPP and solar-induced fluorescence (SIF; a radiance-based indicator of GPP), by capturing structure and radiation  
100 information from a vegetated canopy in field experiments with crops and in numerical experiments. Yet FCVI showed  
101 differences from NIRv due to exposed soil within the vegetated study areas. In previous studies, FCVI and NIRv were  
102 similar for dense green canopies where soils have less of an impact, but this has not yet been tested in the tropics  
103 (Wang et al., 2020; Badgley et al., 2019; Dechant et al., 2020). The product of NDVI and the NIR radiance, called  
104 NIRvrad, was proposed as a proxy for GPP on half-hourly and daily timescales. In contrast, NIRv and FCVI track  
105 changes on longer timescales (Wu et al., 2020; Dechant et al., 2020; Baldocchi et al., 2020; Zeng et al., 2019). Because  
106 the radiance of NIR accounts for incoming radiation at short timescales, NIRvrad has tracked GPP and SIF on half-  
107 hourly and diurnal scales as well as seasonally in crops and, to a limited extent, natural grass and savanna ecosystems  
108 (Dechant et al., 2020; Baldocchi et al., 2020; Zeng et al., 2019; Wu et al., 2020).

109 Readily available UAS-based hyperspectral sensors are capable of robust measurements of NIRv, FCVI, and  
110 NIRvrad at ultra-high spatial scales, i.e. tens of centimeters or less. In this regard, UAS-based data have the potential  
111 to improve our understanding of tropical forest structure and function over a range of scales that are poorly resolved  
112 by other RS platforms. Here, we use high spatial resolution UAS measurements to characterize spatial and temporal  
113 variation in a semi-deciduous tropical forest canopy during the dry season, and compare commonly used spectral

114 indices (NDVI and EVI) to newer vegetation indicators (NIRv, NIRvrad, and FCVI) by (i) examining correlations  
115 between GPP and vegetation indicators using mean values across the canopy throughout the day, (ii) evaluating the  
116 distribution of fine spatial resolution values (~15 cm) across the canopy and examining changes in this spatial variation  
117 throughout the course of two days, and finally (iii) identifying the dominant spatial scale driving variation across our  
118 10 ha study region.

## 119 **2 Materials and Methods**

### 120 **2.1 Study Area**

121 Barro Colorado Island (BCI), Panama, is a 1560 ha island (approximately 15 km<sup>2</sup>) in Gatun Lake, which was formed  
122 by the construction of the Panama Canal. The Smithsonian Tropical Research Institute manages the preserved area  
123 specifically for research. This semi-deciduous moist tropical forest receives approximately 2640 mm mean annual  
124 precipitation and has a mean temperature of 26°C with a dry season from approximately January through April (Detto  
125 et al., 2018). There is high species diversity, with approximately 500 tree species, approximately 60 species per ha,  
126 and about 6.3% of trees at >30cm diameter at breast height (dbh) (Bohman and O'Brien, 2006; Condit et al., 2000).  
127 The UAS and ground measurements were focused on an area approximately 10 ha within the footprint of an eddy  
128 covariance tower near the center of the island (9.156440°, -79.848210°).

### 129 **2.2 Data collection**

130 The GatorEye Unmanned Flying Laboratory is a hardware and software system built for sensor fusion  
131 applications, and which includes hyperspectral, thermal, and visual cameras and a Lidar sensor, coupled with a  
132 differential GNSS, internal hard drives, computing systems, and an Inertial Motion Unit (IMU). Hardware and  
133 processing details, as well as data downloads, are available at [www.gatoreye.org](http://www.gatoreye.org). The GatorEye flew 13 missions on  
134 January 30 and 31, 2019 over the forest canopy within the eddy covariance tower footprint at an average height of 120  
135 m above ground level (AGL) and at 12 m/s (Fig. 1). In this study, we used radiometrically calibrated flight transects  
136 from the Nano VNIR 270 spectral band hyperspectral sensor (Headwall Photonics, Fitchburg, MA, USA) which  
137 covered approximately 1 ha per flight within the EC footprint in this study. The Nano sensor spectrally samples at  
138 approximately 2.2 nm and 12-bit radiometric resolution from 400 to 1050 nm. The frame rate was set to 100 fps, with  
139 an integration time of 12 ms and provided a pixel resolution of approximately 15x15 cm. The Nano was calibrated to  
140 radiance by the manufacturer before the field campaign and pixel drift was removed by dark images collection, which  
141 was corrected for during the conversion from digital number to radiance. The hyperspectral transects were equally  
142 subset for each flight in ENVI + IDL (Harris Geospatial, Boulder, CO). Each flight resulted in 1920 transects of  
143 approximately 400 m length composing three blocks discretized in 2500 data points. Simultaneous lidar was collected  
144 using a VLP-32c ultra puck (Velodyne, San Jose, CA), which was processed to a 0.5x0.5 m resolution digital surface  
145 model (DSM).

146 Turbulent fluxes and meteorological variables were measured from a 40 m Eddy Covariance (EC) flux tower  
147 (Fig. 1). The eddy covariance system includes a sonic anemometer (CSAT3, Campbell Scientific, Logan, UT) and an

148 open-path infrared CO<sub>2</sub>/H<sub>2</sub>O gas analyzer (LI7500, LiCOR, Lincoln, NE). High-frequency (10Hz) measurements  
 149 were acquired by a datalogger (CR1000, Campbell Scientific) and stored on a local PC. Other measurements made at  
 150 the tower include air temperature and relative humidity (HC2S3, Rotronic, Hauppauge New York), and  
 151 photosynthetically active radiation (PAR; BF5, Delta-T Devices, UK). EC data were processed with a custom program  
 152 using a standard routine described in Detto et al. (2010). GPP was derived from daytime values of net ecosystem  
 153 exchange (NEE) by adding the corresponding mean daily ecosystem respiration obtained as the intercept of the light  
 154 response curve (Lasslop et al., 2010). Due to a power issue, EC data were not available during the January 30 flights;  
 155 so only January 31 GPP were available.

156 An HH2 Pro Spectroradiometer (HH2; ASD/Panalytical/Malvern, Boulder, CO) fitted with a diffuse cosine  
 157 receptor was used on the ground in full sun at the forest edge to record incoming irradiance on January 30 and 31,  
 158 2019 (~ 3nm FWHM and spectral sampling at 1nm). HH2 irradiance was resampled to match the Nano hyperspectral  
 159 sensor and used to calculate reflectance. A calibrated reference tarp was placed in full sun at the forest edge and the  
 160 UAS flew over and recorded the tarp each UAS flight. Reflectance was calculated separately using the HH2 and tarp  
 161 data and resulting reflectance values compared as a method to vicariously cross-calibrate reflectance from the  
 162 hyperspectral data (<7.0% difference for all data in the study). In addition, PAR was calculated with the HH2 data and  
 163 compared to the tower-mounted PAR measurement (approximately 1.5 km apart) to help understand any differences  
 164 in the sky conditions during flight times. PAR differences across the site for each flight time for the duration of flights  
 165 (approximately 10-15 minutes in length each) ranged between 4.0% and 10.3%.

166

### 167 **2.3 Vegetation indicators**

168 We calculated NDVI and EVI as (Tucker, 1979; Huete et al., 2002; Rouse JR et al., 1974):

$$169 \quad NDVI = \frac{R_{770-800} - R_{630-670}}{R_{770-800} + R_{630-670}} \quad (1)$$

169 and

$$170 \quad EVI = \frac{2.5(R_{770-800} - R_{630-670})}{R_{770-800} + 6 \times R_{630-670} - 6 \times R_{460-475} + 1} \quad (2)$$

170 where R is reflectance and the subscripts indicate wavelengths. Here, we used the averages of 770-800 nm for NIR,  
 171 630-670 nm for red reflectance, and 460-475 nm for blue bands reflectance and normalized to reduce noise.

172 We further calculated the near-infrared vegetation index NIR<sub>v</sub> as:

$$173 \quad NIR_v = NDVI \times R_{770-800} \quad (3)$$

173 where R<sub>770-800</sub> is the NIR reflectance (Badgley et al., 2017). The fluorescence correction vegetation index (FCVI)  
 174 was calculated from spectral data by subtracting the reflectance in the visible range (R<sub>400-700</sub>) from the NIR  
 175 reflectance (Yang et al., 2020) as follows

$$176 \quad FCVI = R_{770-800} - R_{400-700} \quad (4).$$

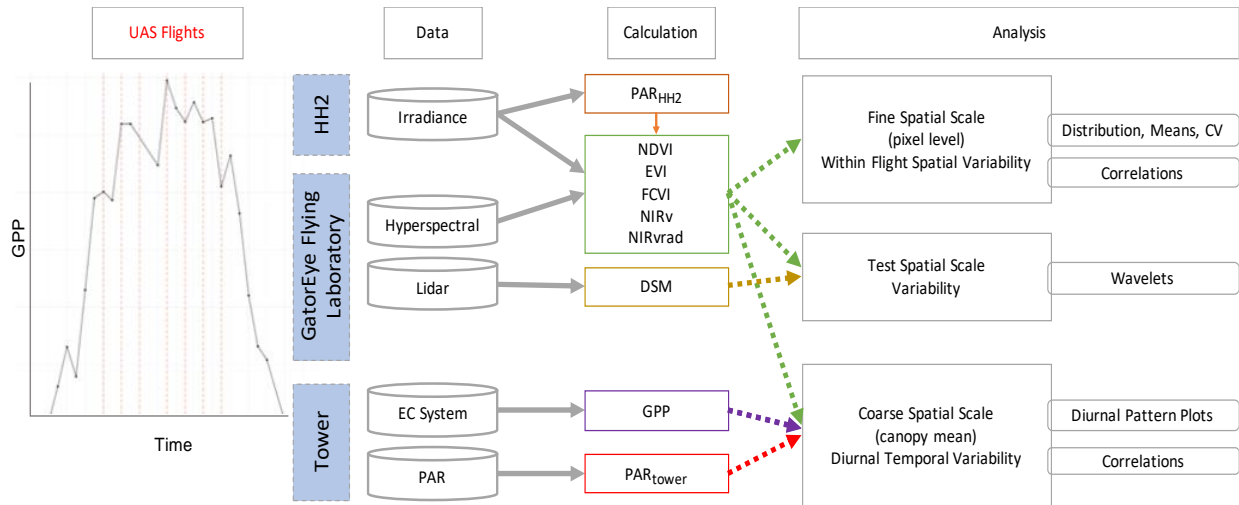
176 The near-infrared radiance of vegetation (NIR<sub>vrad</sub>) was calculated similarly to the NIR<sub>v</sub>, except NDVI was multiplied  
 177 by the radiance, rather than reflectance, from the NIR region (Rad<sub>770-800</sub>) (Wu et al., 2020) as follows:

$$NIRvrad = NDVI \times Rad_{770-800} \quad (5).$$

## 178 2.4 Data Analysis

179 A workflow summarizing data analyses is provided in Fig.1. We examined mean values across the canopy  
180 over the course of one day by creating a diurnal time series of scatterplots of the tower-based PAR data, tower-based  
181 GPP data, and means of all spectral vegetation indicators, on Jan 31, 2019, and ran comparisons using Pearson's  
182 correlation coefficients to examine correlations. Results are provided in Section 3.1 and Fig. 2. At fine spatial scales,  
183 i.e. pixel sizes of ~15 cm, we created density plots, calculated the coefficient of variation (CV), and calculated the  
184 means of all vegetation indicators (NDVI, EVI, NIRv, FCVI, NIRvrad) for each flight to compare spatial and temporal  
185 variability. Results are provided in Section 3.2 and Fig. 3. To determine which spatial scales dominate the variability  
186 of each vegetation quantity, we ran power spectrum wavelet analysis using code created in the Matlab programming  
187 language (Mathworks, Natick, Massachusetts). For each vegetation quantity and each flight, and for the lidar elevation  
188 model representing canopy height, we computed the Morlet wavelet power spectrum of individual transects (Torrence  
189 and Compo, 1998). All power spectra from the wavelet analysis were normalized to unit variance. An ensemble power  
190 spectrum for each vegetation indicator was created by averaging across all the transects of each flight and then across  
191 flights. We then compared the power spectra for each vegetation indicator and lidar data to compare the spatial scales  
192 at which the quantities captured variability as well as the spatial scale at which the lidar-based elevation model  
193 captured variability. Results are provided in Section 3.3 and Fig. 4. For illustration purposes, Fig. S3 is an example of  
194 two synthetic signals generated with fractal Brownian motion algorithm and different level of noise-to-signal ratio  
195 (Signal A and B, respectively, Fig. A1) and the corresponding power spectra which decay differently at smaller spatial  
196 scales (Power Spectra, Fig. A1). Initial UAS data processing was carried out in Interactive Data Language (IDL) and  
197 Environment for Visualizing Images (ENVI) (Harris Geospatial, Boulder, CO). Other analyses, including graphical  
198 illustrations, were carried out using the R open source environment with libraries dplyr, ggplot, and tidyverse (R  
199 Development Core Team, 2010; Wickham et al., 2018; Wickham, 2017, 2016) and Matlab R2019a (Mathworks,  
200 Natick, Massachusetts).

201



202

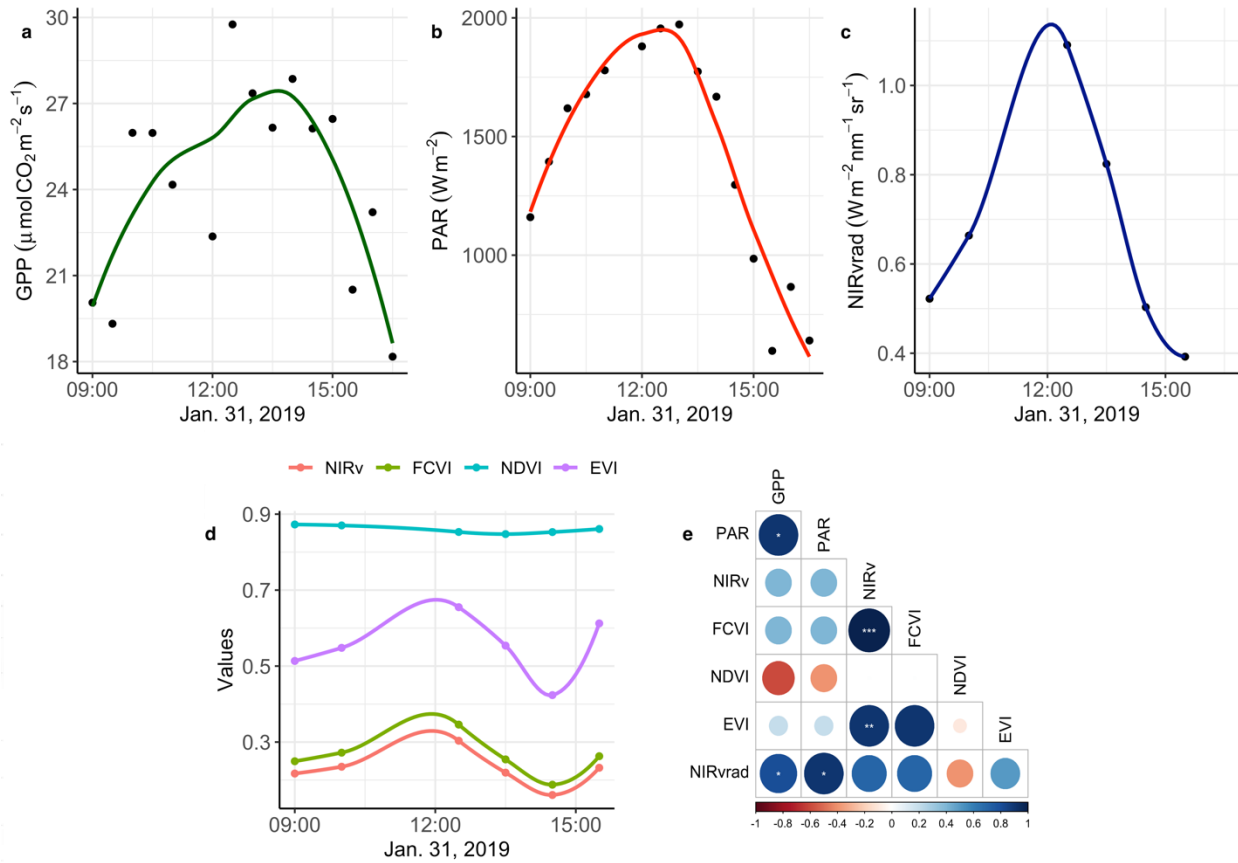
203 **Figure 1.** Summary of methods. Diagram representing discrete flight times for UAS and near-continuous EC-estimated  
 204 GPP (far left). Platforms and instrumentation (blue) consisted of the Analytical Spectral Devices (ASD) Handheld  
 205 Spectroradiometer Pro 2 (HH2), the GatorEye Flying Laboratory, and the tower at Barro Colorado Island (BCI). Data  
 206 collected included irradiance, hyperspectral, Lidar, Eddy Covariance System (EC), and Photosynthetically Active  
 207 Radiation (PAR). Calculations made were PAR with the HH2 (PAR<sub>HH2</sub>), the Normalized Difference Vegetation Index  
 208 (NDVI), Enhanced Vegetation Index (EVI), Fluorescence Correction Vegetation Index (FCVI), the Near Infrared  
 209 Vegetation Index (NIR<sub>v</sub>), the Near Infrared Radiance of Vegetation (NIR<sub>vrad</sub>), the Digital Surface Model (DSM), Gross  
 210 Primary Productivity (GPP) and PAR from the PAR Sensor on the tower (PAR<sub>tower</sub>). An overview of the data analysis at  
 211 each scale is provided in the right of the diagram.

212 **3 Results and discussion**

213 **3.1 Diurnal trend in spectral vegetation indicators, PAR, and GPP**

214 The degree to which remote sensing vegetation indicators represent changes in GPP depend largely on canopy  
 215 structure-dependent light absorption and scattering processes, that is, exploiting relationships between a remote  
 216 sensing vegetation quantity, PAR or APAR, and GPP. Fig. 2 shows GPP, PAR, and the mean value of each vegetation  
 217 quantity at each flight time over the course of January 31, the day on which we had overlapping data between the UAS  
 218 and eddy covariance system (Fig. 2a-d). Additionally, Pearson correlation coefficients among mean NIR<sub>v</sub>, FCVI,  
 219 NIR<sub>vrad</sub>, EVI, and NDVI for each flight time and the GPP and PAR values at the flight times are shown in Fig. 2d.  
 220 NIR<sub>v</sub> is significantly and strongly positively correlated to both FCVI ( $r=0.9$ ,  $p<0.001$ ) and EVI ( $r=0.9$ ,  $p<0.01$ ).  
 221 NIR<sub>vrad</sub> is the only vegetation quantity with a significant correlation to PAR and GPP, with a strong positive  
 222 relationship (0.9 and 0.81, respectively,  $p$ -values  $<0.05$ ; Fig. 2d). Mean NIR<sub>vrad</sub> values also have the greatest relative  
 223 diurnal change among the vegetation indicators (Fig. 2c and d). These results demonstrate that a shared correlation of  
 224 NIR<sub>vrad</sub> and GPP to PAR results in mean NIR<sub>vrad</sub> tracking diurnal changes in GPP to a greater degree than NIR<sub>v</sub>,  
 225 FCVI, NDVI or EVI, because NIR<sub>vrad</sub> takes incoming radiation into account whereas the other vegetation indicators  
 226 do not. The ability of NIR<sub>vrad</sub> to track APAR is notable alone. However, our evidence supports the proposed use of  
 227 NIR<sub>vrad</sub> as a proxy for changes in GPP on short timescales – albeit based on only one day of data. NIR<sub>vrad</sub> is a more  
 228 practical proxy of GPP than SIF in the sense that a separate instrument to measure PAR is not needed (Wu et al., 2020;  
 229 Zeng et al., 2019). Given that the relationship between NIR<sub>vrad</sub> and GPP depends on PAR, it is unclear if the

230 association between NIRvrad and GPP would weaken during the wet season when low light or diffuse light conditions  
 231 are more common (Berry and Goldsmith, 2020).



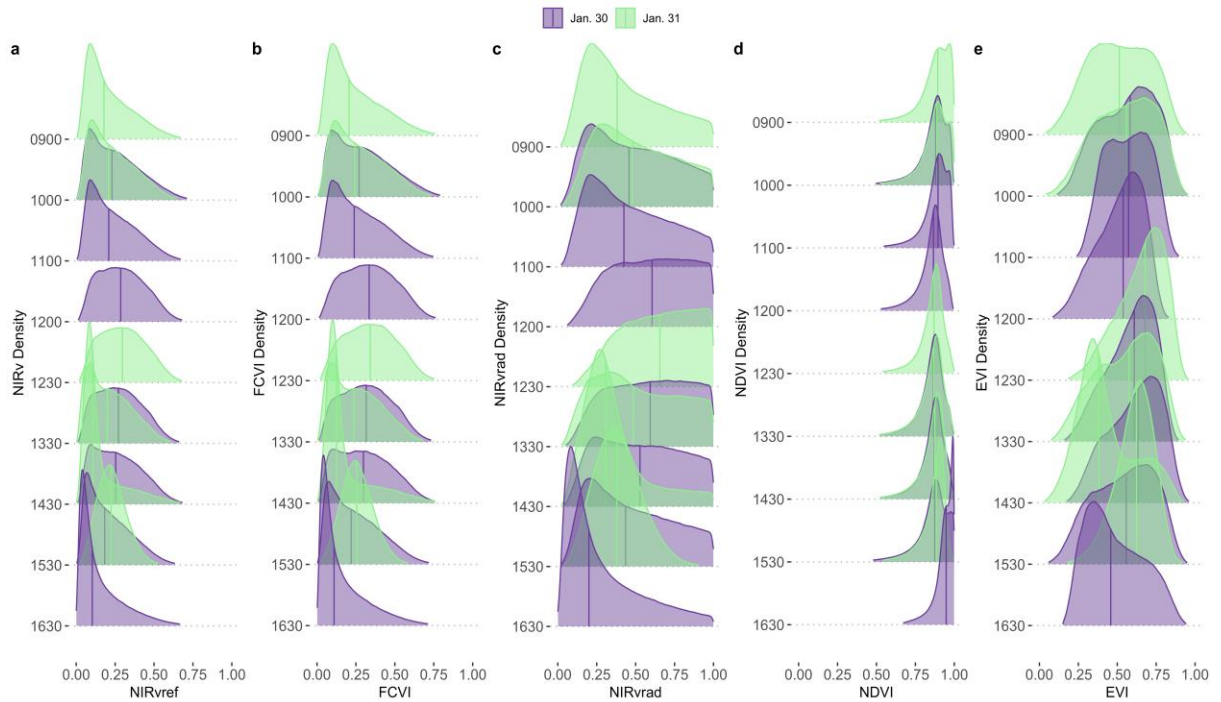
232  
 233 **Fig. 2. Diurnal time series smoothed with a LOESS filter of a) GPP b) PAR c) NIRvrad d) NIRv, FCVI, NDVI, and EVI e)**  
 234 **comparisons of quantities using Pearson correlations color indicates strength of relationship, \* = p-value<0.05, \*\* = p-value**  
 235 **<0.01, \*\*\* = p-value <0.001.**

236 **3.2 Tropical forest canopy variation**

237 Spatial distributions and the coefficient of variation (CV) of all pixels of NIRv, FCVI, and NIRvrad are  
 238 generally similar to one another and show considerable variation spatially across the canopy and temporally over the  
 239 course of a day and across days (Fig. 3a-c, Table A2). NIRv, FCVI, and NIRvrad distributions are distinct from EVI  
 240 and NDVI (Fig. 3a-e, Table A2, and Table A2). NIRv, FCVI, and NIRvrad have the highest CV at each flight time  
 241 (between 39.78% and 91.54%, Table A1), followed by EVI (between 20.24% and 37.24%, Table A2) and NDVI  
 242 varied the least at any flight time (between 9.83% and 12.82%, Table A2). For some indices, mean values across the  
 243 canopy fail to capture extreme high (NIRv, NIRvrad, and FCVI) or low values (NDVI) during morning and afternoon  
 244 hours. This pattern suggests “hot” and “cool” spots of activity related to heterogeneity in forest structure and low sun  
 245 angles. In previous studies, the directional effects on NIRv have been examined on coarse spatial scales (i.e. satellites)  
 246 and have been proposed as a means of improving understanding of NIRv agreement to GPP (Hao et al., 2021; Dechant  
 247 et al., 2020; Baldocchi et al., 2020; Zhang et al., 2020). Our results demonstrate that NIRv, FCVI, and NIRvrad capture  
 248 fine-grained heterogeneity of this tropical forest canopy, which was obscured by EVI and NDVI (Fig. 3a-e). NIRv

249 and NIRvrad use NDVI, thus, by definition, NIR is the largest contributing factor to the heterogeneity captured (Fig.  
250 3a, c, and e). While NIRv and NIRvrad distributions are generally similar, they diverge in the afternoons when PAR  
251 declines, which likely is why NIRvrad is better correlated with GPP. EVI variability was higher than NDVI variability,  
252 but lower than that of NIRv, FCVI, and NIRvrad, indicating that EVI has a different level of sensitivity to viewing  
253 geometry and canopy components (potentially understory), light absorption and scattering regime of the canopy than  
254 the other indices (Table A1 and Table A2). We also show empirically that NIRv and FCVI are virtually the same in a  
255 dense tropical forest presumably due to both indices similarly representing the radiation regime of the tropical forest  
256 canopy, i.e. light capture and scattering, in conditions with little background soil, supporting the predictions of earlier  
257 studies (Dechant et al., 2020; Zeng et al., 2019; Yang et al., 2018b; Wu et al., 2020).

258 Midday distributions of NIRv, FCVI, and NIRvrad on Jan. 30 at 1200 and 1330 and Jan. 31 at 1230 are less  
259 skewed than at other times of the day whereas morning and afternoon distributions are skewed toward lower values,  
260 except for Jan. 31 at 1530 (Fig. 3a-c). On both days, when mean values peak at midday, the variation for all vegetation  
261 indicators is lowest (Jan 30, 1200 CV between 47.6 and 49.2 and Jan 31, 1230 CV between 45.6 and 47.2) (Fig. 3,  
262 Table A1). The highest variability occurred in the afternoon on both days (Jan 30, 1630 CV between 91.3% and 91.5  
263 and Jan 31, 1430 CV between 83.3% and 83.8% for all quantities) (Fig. 3, Table A2). At midday, NIRv, FCVI, and  
264 NIRvrad variability was low and means were high, indicating that viewing and sun geometry drive the higher and  
265 lower values during morning and afternoon. This effect is greater in the afternoon than the morning (Fig. 3, Table  
266 A2). However, a different pattern is apparent on Jan. 31 during the 1530 flight time when mean values increased from  
267 the 1430 flight time means and the CV values were the lowest of any flight observations in the study and this influence  
268 appears to be greatest on EVI. It is possible that this was due to another type of effect on illumination geometry, such  
269 as wind influencing the UAS, diffuse radiation effects, or hotspot effects.



270

271

272

**Fig. 3. NIRv (a), FCVI (b), and NIRvrad (c) density plots for each flight time on January 30 and January 31, 2019. Colours of distributions indicate day.**

273

### 3.3 Power Spectrum Analysis

274

275

276

277

278

279

280

281

282

Power spectrum analysis was used to identify the dominant spatial scales driving variability across the canopy (Fig. 4). In Fig. 4, the area beneath the curve is proportional to the variance because it is the spectrum divided by the corresponding scale and then plotted as a function of the log of the scale (example signals and power spectra provided Fig. A1). Similar to their spatial distributions (Fig. 3), NIRvrad and FCVI are indistinguishable in their dominant scales of spatial variability (Fig. 3) (Dechant et al., 2020; Zeng et al., 2019). Power spectrum analysis shows a distinct peak around 50 m spatial scale for NIRv, NIRvrad, FCVI, and EVI, whereas NDVI peaks at approximately 90 m. The largest tree crown sizes on BCI are on the order of 20-30 m in diameter and the most common crown sizes are between 4-10 m (Fig. A2). Thus, the spatial variability of the vegetation indicators is strongly influenced by larger forest structures, such as forest gaps and tree clusters, rather than individual tree crowns.

283

284

285

286

287

288

289

290

291

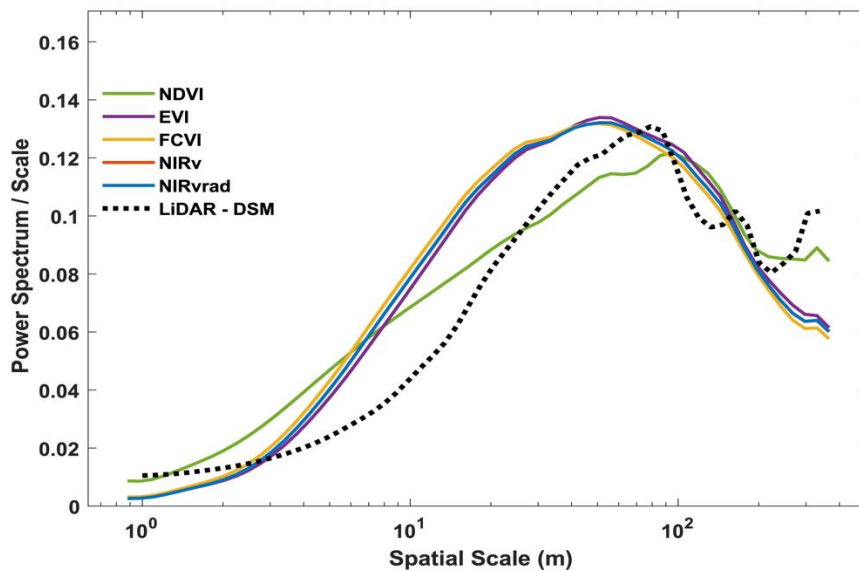
This larger scale of variability is also confirmed by the power spectrum of the lidar-derived canopy surface model, which displays a peak at 70 m scale, indicating that larger than tree crown scales produce the most variability in canopy height. In other words, UAS-based lidar data also show that canopy heights within a 70 m spatial scale create strong spatial features on the landscape. Vegetation indicators and the lidar canopy surface model appear less effective at capturing smaller scale differences within a canopy (leaves or leaf clumps) or among the most frequent tree crown sizes on BCI (4-10 m sunlit tree crown sizes determined by stereophotos; Fig. A2). However, the peaks in the vegetation indicators are broader than the peak in the lidar data, showing that smaller features of the canopy are still contributing to the total spatial signal in the power spectra. These results suggest that satellite data with a spatial resolution greater than ~50 m may miss important variation in diverse tropical forest canopies. NDVI displays a

292 different shape with a slower decay at small scales, indicating less distinguishable spatial structures from the canopy,  
293 and a peak shifted to the larger scales (Fig. 4), i.e. NDVI does not distinguish smaller spatial structures. At much larger  
294 scales (>100-200 m), the vegetation indicators decline smoothly, while NDVI and especially lidar show an increase  
295 in variance probably associated with topographic heterogeneity.

296 One reason why vegetation indicators and LiDAR captured variability at spatial scales larger than the most  
297 common tree crown sizes on BCI is that canopy heights tend to be more uniform on BCI compared to other tropical  
298 forests, possibly due to wind (Bohlman and O'Brien, 2006). For example, Dipterocarpus dominated South-East Asian  
299 forests have emergent trees, unlike BCI, which can reach up to 60 m in height. Additionally, tree crowns on BCI tend  
300 to be more flat-topped than conical or rounded, and trees can be found clumped in similar heights, which could explain  
301 why the most often detected unit is larger than the mean of a single crown. On the other end of the spectrum, forest  
302 gaps can be larger than a single crown because treefall often affects neighbouring trees.

303 Vegetation indicators and the Lidar-derived surface model represent the spectral and structural properties most  
304 broadly of the upper canopy, and thus it is conceivable that they display similar spatial variability. However, NIRv,  
305 FCVI, NIRvrad, and EVI discriminated details at a different spatial scale from NDVI and LiDAR. These results  
306 parallel the variability detected in their distributions (Fig. 3 and Table A1), where NDVI patterns were distinct from  
307 the other vegetation indicators. Taken together, these results show that NIRv, FCVI, and NIRvrad have a smoother  
308 spatial pattern and peak at finer scales than NDVI, which is known to saturate at high green biomass (Zhu and Liu,  
309 2015; Huete et al., 2002), whereas NIRv, FCVI, and NIRvrad should better correlate with aspects of photosynthetic  
310 capacity. Thus, these emerging indicators should measure finer resolution spatial heterogeneity and should be more  
311 adept at monitoring changes in structure and function of the canopy than NDVI. Additionally, the emerging indicators  
312 can potentially disaggregate the physiological and structural component of SIF when SIF measurements are available  
313 since changes in structure of the forest coincide with changes in GPP (Wang et al., 2020; Wu et al., 2020; Yang et al.,  
314 2020; Dechant et al., 2020). Emerging indicators' heightened ability to differentiate the fine-scale spatial variability  
315 in the canopy is likely due to the influence of high upwelling of NIR from the canopy and understory, particularly in  
316 the dry season, which tend to blur the signal of the upper canopy for NDVI. Notably, EVI and NDVI, two common  
317 indicators of vegetation greenness, show differences in their power spectrum, in particular the slope of the curve for  
318 scales less than 20 m. EVI was designed to better capture vegetation changes by exploiting variability in the reflectance  
319 in the blue range, especially effective in dense green canopies. This may help explain the scale of variability in this  
320 canopy where variation in the blue may be expected to manifest, especially because deciduous crowns, which have  
321 high reflectance in blue wavelengths compared to fully leaved crowns, are present on BCI (Bohlman, 2008).

322



323

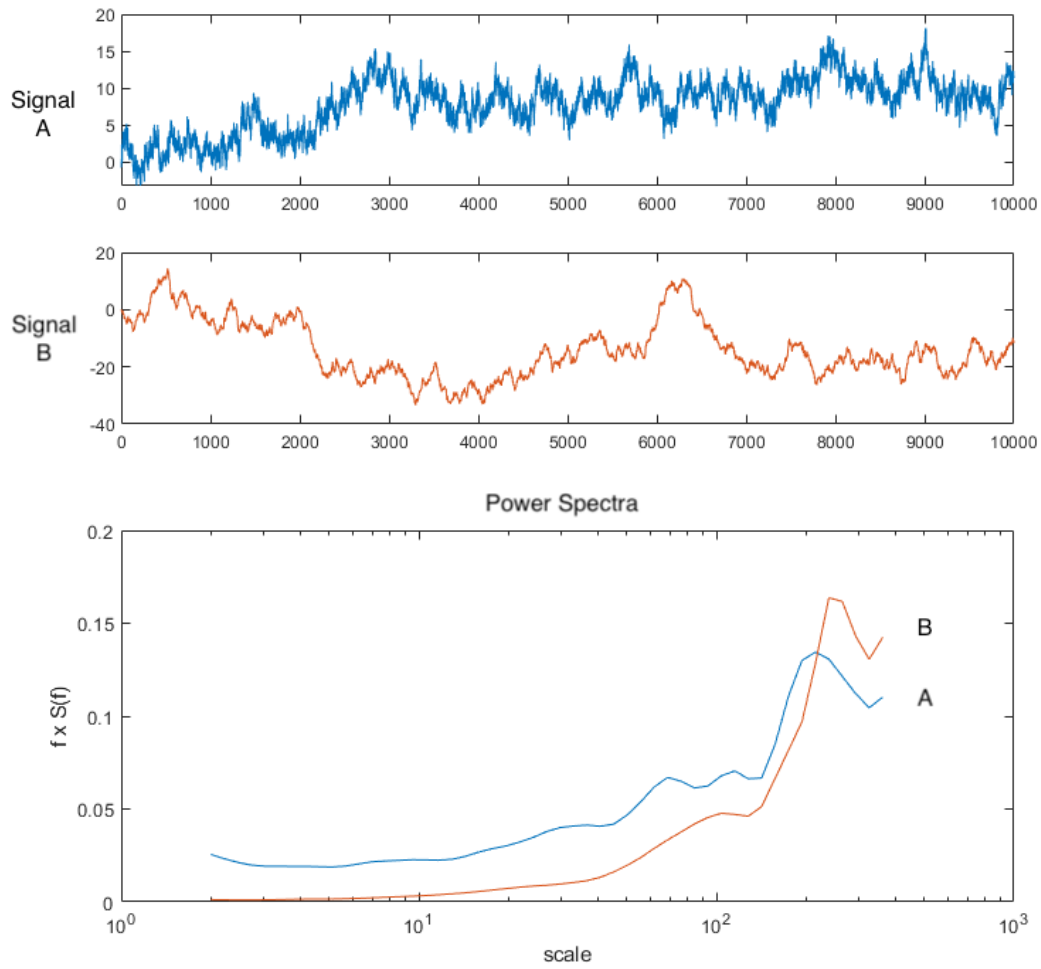
324 **Fig. 4. Ensemble wavelet power spectra for all the quantities used in this study and a LiDAR-derived digital**  
 325 **surface model (DSM). Note that FCVI and NIRv are similar, thus the NIRv curve is obscured by the FCVI.**  
 326 **Ensembles were created by averaging the spectrum of individual transects, then averaging across flights. Note**  
 327 **that in this representation, the spectrum divided by the corresponding scale as a function of the log of the scale,**  
 328 **the area beneath the curve is proportional to the variance.**

#### 329 4 Conclusions

330 We examined NIRv, FCVI, and NIRvrad, emerging vegetation indicators related to fPAR of a semi-deciduous  
 331 tropical forest canopy using UAS-based hyperspectral data. Our findings demonstrate that NIRvrad has greater  
 332 potential to track GPP over the course of a day than the non-radiance-based indices as evidenced by a shared  
 333 correlation among NIRvrad, PAR, and GPP. Thus, NIRvrad is a potential proxy for tracking GPP on short timescales  
 334 without the need for separate measurements of incoming irradiance. Also, NIRv, FCVI, and NIRvrad at high spatial  
 335 resolution (~15cm) unveil greater spatial and diurnal variability of BCI's tropical forest canopy versus EVI or NDVI,  
 336 which may pave the way to improve our understanding of the relationship between GPP and remote sensing  
 337 observations. For instance, by benchmarking changes of vegetation function and structure that underlie a GPP  
 338 measurement representing the whole EC footprint, fine scale NIRv, FCVI, or NIRvrad measurements may reveal  
 339 highly differential behaviors of tropical species diurnally to seasonally. The dominant scale driving spatial variability  
 340 of spectral measurements and lidar data are larger forest structures occurring on BCI, such as groups of similar trees  
 341 or forest gaps. Yet, smaller, broader peaks in the power spectra of NIRv, FCVI, NIRvrad, and EVI indicate these four  
 342 indices incorporate smaller scale information compared to NDVI. Taken together, the demonstrated potential to track  
 343 GPP, measure spatial heterogeneity and variability, and capture forest structural characteristics of BCI open greater  
 344 possibilities to examine structure and function within and across this tropical forest.

345 Because remote sensing advancements are making it possible to capture physiological responses of vegetation,  
 346 the importance of improved techniques to examine the radiation regime, for instance estimating fPAR or APAR, can

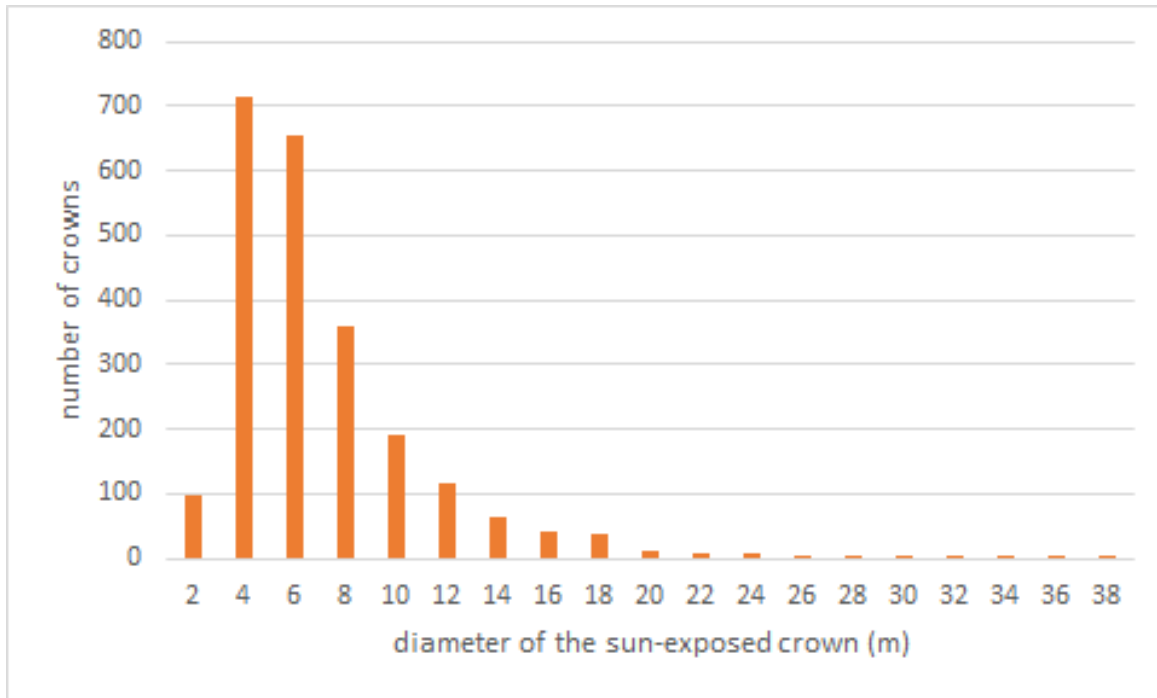
347 be overlooked. However, recent studies have highlighted the importance and difficulties of measuring fPAR and  
348 APAR, the strong dependence of measurements on illumination and viewing geometry, as well as the need for  
349 increased understanding of structure-related radiation regime information more generally e.g. (Hao et al., 2021;  
350 Dechant et al., 2020; Baldocchi et al., 2020; Rocha et al., 2021; Zhang et al., 2020). For NIRv, FCVI, and NIRvrad,  
351 inclusion of the NIR spectral region makes the emerging indices more sensitive to incoming, absorbed, and scattered  
352 radiation, which can be influenced by illumination and viewing geometry, changes in canopy leaf angles or associated  
353 structure changes. In the case of NIRvrad, which was most strongly associated with GPP, changes in light regime and  
354 associated photosynthetic capacity can even be captured diurnally. Furthermore, NIRv, FCVI, and NIRvrad  
355 measurements, especially at high spatial and temporal resolution can help inform our understanding of one another,  
356 traditional reflectance-based indices, and other measurements such as SIF. This study highlights the importance of  
357 understanding the incoming solar radiation, absorbed and scattered radiation, and illumination and viewing geometry  
358 of any remote sensing data, but it also encourages exploiting RS observations to improve our ability to measure  
359 structure-related light capture and scattering patterns. It is in this role, we show these measurements should be further  
360 investigated as valuable tools to improve our understanding of complex tropical forest canopies and potentially as an  
361 improved estimate of fPAR, APAR, or GPP. While this study focuses on BCI, these techniques could be applied more  
362 broadly for the purposes of defining the dominant scale of spatial variability, tracking structural changes, monitoring  
363 coincident changes in GPP or light regime, or as inputs to vegetation models of tropical forest structure and function.



365

366 **Figure A1.** Sample signals with relatively higher noise (Signal A) and lower noise (Signal B) and their corresponding  
 367 Power Spectra ensemble plotted as normalized on log scale. Note the representation of the variance by area under the curve  
 368 is preserved by multiplying the Power ( $S(f)$ ) by the frequency ( $f$ ). In this way the area beneath the curve is still proportional  
 369 to the variance.

370



371  
 372 **Figure A2.** Distribution of tree crown sizes on BCI in a sample ~10 ha plot taken from digitized high spatial resolution  
 373 stereo photos that were linked to stems in the field (Bohman and Pacala 2012). This ~10 ha plot does not coincide with the  
 374 ~10 ha area sampled by the UAS near the eddy covariance tower in this study.

375  
 376 **Table A1.** Mean, standard deviation (Sdev) and coefficient of variation (CV) of NIRv, NIRvrad, and FCVI measurements  
 377 for the study.

378

Flight Time	Mean	SDev	CV	Mean	SDev	CV	Mean	SDev	CV
	NIRv	NIRv	NIRv (%)	NIRvrad	NIRvrad	NIRvrad (%)	FCVI	FCVI	FCVI (%)
Jan30_1000	0.26	0.16	61.36	0.60	0.36	60.54	0.29	0.18	59.69
Jan30_1100	0.24	0.15	61.48	0.54	0.33	60.56	0.27	0.16	60.89
Jan30_1200	0.29	0.15	49.20	0.82	0.39	47.59	0.34	0.16	47.88
Jan30_1330	0.28	0.14	50.46	0.81	0.40	49.24	0.32	0.16	49.16
Jan30_1430	0.27	0.15	55.46	0.70	0.38	54.38	0.31	0.17	54.22
Jan30_1530	0.21	0.14	65.10	0.63	0.41	64.71	0.25	0.16	64.01
Jan30_1630	0.16	0.14	91.54	0.32	0.30	91.54	0.17	0.15	91.39
Jan31_0900	0.22	0.14	66.31	0.52	0.34	65.25	0.25	0.16	66.01
Jan31_1000	0.24	0.14	59.43	0.66	0.39	58.29	0.27	0.16	59.04
Jan31_1230	0.30	0.14	47.17	1.09	0.50	45.63	0.35	0.16	45.91
Jan31_1330	0.22	0.14	61.91	0.82	0.51	61.47	0.25	0.15	60.53
Jan31_1430	0.16	0.14	85.32	0.50	0.42	83.81	0.19	0.16	83.83

Jan31_1530	0.86	0.08	9.83	0.61	0.12	20.24	0.53	0.04	8.15
------------	------	------	------	------	------	-------	------	------	------

379  
380  
381

**Table A2. Mean, standard deviation (Sdev) and coefficient of variation (CV) of NDVI and EVI measurements for the study.**

Flight Time	Mean NDVI	SDev NDVI	CV NDVI (%)	Mean EVI	SDev EVI	CV EVI (%)
Jan30_1000	0.86	0.10	11.64	0.57	0.18	31.54
Jan30_1100	0.88	0.09	10.15	0.57	0.14	24.40
Jan30_1200	0.85	0.09	10.38	0.52	0.15	28.48
Jan30_1330	0.85	0.09	10.60	0.59	0.15	25.24
Jan30_1430	0.85	0.09	10.35	0.61	0.16	26.84
Jan30_1530	0.85	0.11	12.52	0.54	0.19	35.21
Jan30_1630	0.93	0.06	6.69	0.49	0.18	36.90
Jan31_0900	0.87	0.10	11.54	0.51	0.19	37.24
Jan31_1000	0.87	0.10	11.08	0.55	0.19	34.66
Jan31_1230	0.85	0.08	9.82	0.66	0.15	22.72
Jan31_1330	0.85	0.09	10.70	0.55	0.19	33.80
Jan31_1430	0.85	0.09	10.58	0.42	0.18	43.07
Jan31_1530	0.86	0.08	9.83	0.61	0.12	20.24

382  
383  
384  
385  
386

387 ***Code availability***

388 ***Data availability***

389 GatorEye data related to this project can be downloaded from [www.gatoreye.org](http://www.gatoreye.org). Code and other material  
390 with links provided upon request.

391

392 ***Author contributions***

393 T.M. designed the study with the help of S.P. and S.A.B.. M.D. and T.M. outfitted the tower and collected tower-  
394 based data, T.M. and E.N.B. collected the UAS data. E.N.B., A.M.A.Z., and T.M. pre-processed the hyperspectral and  
395 lidar data. T.M. and M.D. further processed UAV, lidar, and GPP data and ran data analysis. M.D., S.P., S.A.B., C.S.,  
396 contributed with the methodological framework, data processing analysis and write up T.M., M.D., S.P., S.A.B., C.S.,

397 E.N.B., and A.M.A.Z. contributed to the interpretation, quality control and revisions of the manuscript. All authors  
398 read and approved the final version of the manuscript.

### 399 *Competing interests*

400 The authors declare no conflict of interest.

### 401 *Acknowledgments*

402 This project execution was carried out while T.M., the primary author, was a Provost's Postdoctoral Fellow  
403 in the Department of Geography at Florida State University under the advisement of S.P.. T.M. wishes to extend the  
404 sincerest thanks to S.P. for support and guidance, as well as to the FSU Department of Geography, FSU Provost's  
405 Postdoctoral Fellows program, and to co-authors who served as mentors. Support for this project, including portions  
406 of field logistic and data collection costs and materials, and support for T.M., was provided by the Provost's  
407 Postdoctoral Fellows Program at Florida State University. E.N.B. was supported through the School of Forest,  
408 Fisheries and Geomatics Sciences and expenses and data collection paid for by T.M.'s Provost's Postdoctoral Fellows  
409 Program at Florida State University, A.M.A.Z through the Center for Latin American Studies, and hardware, software,  
410 and system costs associated with the GatorEye and data collection were provided through the McIntire Stennis  
411 Program of the USDA and the School of Forest, Fisheries and Geomatics Sciences. M.D. was supported by the Carbon  
412 Mitigation Initiative at Princeton University. The authors wish to thank the vast support of the collaborators, staff, and  
413 researchers at the Smithsonian Tropical Research Institute and, specifically at Barro Colorado Island, without which  
414 this research would not be possible. Among other contributors to the work, we also extend special thanks to Alfonso  
415 Zambrano, Carli Merrick, Riley Fortier, and Pete Kerby-Miller for field work assistance, and Dr. S. Joseph Wright  
416 and Dr. Helene Muller-Landau for support on site as well.

417

### 418 **References**

- 419 Alonso, L., Moreno, J., Moya, I., and R. Miller, J. R.: A Comparison of Different Techniques for Passive Measurement  
420 of Vegetation Photosynthetic Activity: Solar-Induced Fluorescence, Red-Edge Reflectance Structure and  
421 Photochemical Reflectance Indices, *IEEE*, 3, 2003.
- 422 Alonso, L., Gómez-Chova, L., Vila-Francés, J., Amorós-López, J., Guanter, L., Calpe, J., and Moreno, J.: Sensitivity  
423 analysis of the Fraunhofer Line Discrimination method for the measurement of chlorophyll fluorescence using a field  
424 spectroradiometer, *IEEE*, 4, 2007.
- 425 Alonso, L., Gómez-Chova, L., Vila-Francés, J., Amorós-López, J., Guanter, L., Calpe, J., and Moreno, J.: Improved  
426 Fraunhofer Line Discrimination Method for Vegetation Fluorescence Quantification, *IEEE GEOSCIENCE AND  
427 REMOTE SENSING LETTERS*, 5, 5, 2008.
- 428 Badgley, G., Field, C. B., and Berry, J. A.: Canopy near-infrared reflectance and terrestrial photosynthesis, *Sci Adv*,  
429 3, e1602244, 10.1126/sciadv.1602244, 2017.
- 430 Badgley, G., Anderegg, L. D. L., Berry, J. A., and Field, C. B.: Terrestrial gross primary production: Using NIRV to  
431 scale from site to globe, *Glob Chang Biol*, 25, 3731-3740, 10.1111/gcb.14729, 2019.
- 432 Baldocchi, D. D., Ryu, Y., Dechant, B., Eichelmann, E., Hemes, K., Ma, S., Rey Sanchez, C., Shortt, R., Szutu, D.,  
433 Valach, A., Verfaillie, J., Badgley, G., Zeng, Y., and Berry, J. A.: Outgoing Near Infrared Radiation from Vegetation  
434 Scales with Canopy Photosynthesis Across a Spectrum of Function, Structure, Physiological Capacity and Weather,  
435 *Journal of Geophysical Research: Biogeosciences*, 10.1029/2019jg005534, 2020.

436 Berry, Z. C., & Goldsmith, G. R.: Diffuse light and wetting differentially affect tropical tree leaf photosynthesis. *New*  
437 *Phytologist*, 225(1), 143-153, 10.1111/nph.16121,2020.

438 Bohlman, Stephanie. "Hyperspectral remote sensing of exposed wood and deciduous trees in seasonal tropical  
439 forests." In *Hyperspectral remote sensing of tropical and subtropical forests*, pp. 177-192. CRC Press, 2008.

440 Kalacska, M., & Sanchez-Azofeifa, G. A. (Eds.)  
441  
442

443 Bohlman, S. and O'Brien, S.: Allometry, adult stature and regeneration requirement of 65 tree species on Barro  
444 Colorado Island, Panama, *Journal of Tropical Ecology*, 22, 123-136, 10.1017/s0266467405003019, 2006.

445 Bohlman, S. and Pacala, S.: A forest structure model that determines crown layers and partitions growth and mortality  
446 rates for landscape-scale applications of tropical forests, *Journal of Ecology*, 100, 508-518, 10.1111/j.1365-  
447 2745.2011.01935.x, 2012.

448 Castro, A. O., Chen, J., Zang, C. S., Shekhar, A., Jimenez, J. C., Bhattacharjee, S., Kindu, M., Morales, V. H., and  
449 Rammig, A.: OCO-2 Solar-Induced Chlorophyll Fluorescence Variability across Ecoregions of the Amazon Basin  
450 and the Extreme Drought Effects of El Niño (2015–2016), *Remote Sensing*, 12, 10.3390/rs12071202, 2020.

451 Clark, D. B., Olivas, P. C., Oberbauer, S. F., Clark, D. A., and Ryan, M. G.: First direct landscape-scale measurement  
452 of tropical rain forest Leaf Area Index, a key driver of global primary productivity, *Ecol Lett*, 11, 163-172,  
453 10.1111/j.1461-0248.2007.01134.x, 2008.

454 Clark, D. A., Asao, S., Fisher, R., Reed, S., Reich, P. B., Ryan, M. G., Wood, T. E., and Yang, X.: Reviews and  
455 syntheses: Field data to benchmark the carbon cycle models for tropical forests, *Biogeosciences*, 14, 4663-4690,  
456 10.5194/bg-14-4663-2017, 2017.

457 Cogliati, S., Verhoef, W., Kraft, S., Sabater, N., Alonso, L., Vicent, J., Moreno, J., Drusch, M., and Colombo, R.:  
458 Retrieval of sun-induced fluorescence using advanced spectral fitting methods, *Remote Sensing of Environment*, 169,  
459 344-357, 10.1016/j.rse.2015.08.022, 2015.

460 Condit, R. S., Watts, K., Bohlman, S., Perez, R., Foster, R. B., and Hubbell, S. P.: Quantifying the deciduousness of  
461 tropical forest canopies under varying climates, *Journal of Vegetation Science*, 11, 10, 2000.

462 Dechant, B., Ryu, Y., Badgley, G., Zeng, Y., Berry, J. A., Zhang, Y., Goulas, Y., Li, Z., Zhang, Q., Kang, M., Li, J.,  
463 and Moya, I.: Canopy structure explains the relationship between photosynthesis and sun-induced chlorophyll  
464 fluorescence in crops, *Remote Sensing of Environment*, 241, 10.1016/j.rse.2020.111733, 2020.

465 Detto, M., Baldocchi, D., and Katul, G. G.: Scaling Properties of Biologically Active Scalar Concentration  
466 Fluctuations in the Atmospheric Surface Layer over a Managed Peatland, *Boundary-Layer Meteorology*, 136, 407-  
467 430, 10.1007/s10546-010-9514-z, 2010.

468 Detto, M., Wright, S. J., Calderon, O., and Muller-Landau, H. C.: Resource acquisition and reproductive strategies of  
469 tropical forest in response to the El Niño-Southern Oscillation, *Nature communications*, 9, 913, 10.1038/s41467-018-  
470 03306-9, 2018.

471 Frankenberg, C., Fisher, J. B., Worden, J. R., Badgley, G., Saatchi, S. S., Lee, J. E., Toon, G. C., Butz, A., Jung, M.,  
472 Kuze, A., and Yokota, T.: New global observations of the terrestrial carbon cycle from GOSAT: Patterns of plant  
473 fluorescence with gross primary productivity, *Geophysical Research Letters*, 38, 10.1029/2011gl048738, 2011.

474 Gamon, J. A., Kovalchuck, O., Wong, C. Y. S., Harris, A., and Garrity, S. R.: Monitoring seasonal and diurnal changes  
475 in photosynthetic pigments with automated PRI and NDVI sensors, *Biogeosciences*, 12, 4149-4159, 10.5194/bg-12-  
476 4149-2015, 2015.

477 Gao, W., Kim, Y., Ustin, S. L., Huete, A. R., Jiang, Z., and Miura, T.: Multisensor reflectance and vegetation index  
478 comparisons of Amazon tropical forest phenology with hyperspectral Hyperion data, *Remote Sensing and Modeling*  
479 *of Ecosystems for Sustainability IV*, 10.1117/12.734974, 2007.

480 Gelybó, G., Barcza, Z., Kern, A., and Kljun, N.: Effect of spatial heterogeneity on the validation of remote sensing  
481 based GPP estimations, *Agricultural and Forest Meteorology*, 174-175, 43-53, 10.1016/j.agrformet.2013.02.003,  
482 2013.

483 Glenn, E. P., Huete, A. R., Nagler, P. L., and Nelson, S. G.: Relationship Between Remotely-sensed Vegetation  
484 Indices, Canopy Attributes and Plant Physiological Processes: What Vegetation Indices Can and Cannot Tell Us About  
485 the Landscape, *Sensors*, 8, 24, 2008.

486 Guan, K., Pan, M., Li, H., Wolf, A., Wu, J., Medvigy, D., Caylor, K. K., Sheffield, J., Wood, E. F., Malhi, Y., Liang,  
487 M., Kimball, J. S., Saleska, Scott R., Berry, J., Joiner, J., and Lyapustin, A. I.: Photosynthetic seasonality of global  
488 tropical forests constrained by hydroclimate, *Nature Geoscience*, 8, 284-289, 10.1038/ngeo2382, 2015.

489 Guanter, L., Frankenberg, C., Dudhia, A., Lewis, P. E., Gómez-Dans, J., Kuze, A., Suto, H., and Grainger, R. G.:  
490 Retrieval and global assessment of terrestrial chlorophyll fluorescence from GOSAT space measurements, *Remote*  
491 *Sensing of Environment*, 121, 236-251, 10.1016/j.rse.2012.02.006, 2012.

492 Guanter, L., Zhang, Y., Jung, M., Joiner, J., Voigt, M., Berry, J. A., Frankenberg, C., Huete, A. R., Zarco-Tejada, P.,  
493 Lee, J. E., Moran, M. S., Ponce-Campos, G., Beer, C., Camps-Valls, G., Buchmann, N., Gianelle, D., Klumpp, K.,  
494 Cescatti, A., Baker, J. M., and Griffis, T. J.: Global and time-resolved monitoring of crop photosynthesis with  
495 chlorophyll fluorescence, *Proceedings of the National Academy of Sciences of the United States of America*, 111,  
496 E1327-1333, 10.1073/pnas.1320008111, 2014.

497 Hao, D., Asrar, G. R., Zeng, Y., Yang, X., Li, X., Xiao, J., Guan, K., Wen, J., Xiao, Q., Berry, J. A., and Chen, M.:  
498 Potential of hotspot solar-induced chlorophyll fluorescence for better tracking terrestrial photosynthesis, *Glob Chang*  
499 *Biol.*, 10.1111/gcb.15554, 2021.

500 Heinsch, F. A., Maosheng, Z., Running, S. W., Kimball, J. S., Nemani, R. R., Davis, K. J., Bolstad, P. V., Cook, B.  
501 D., Desai, A. R., Ricciuto, D. M., Law, B. E., Oechel, W. C., Hyojung, K., Hongyan, L., Wofsy, S. C., Dunn, A. L.,  
502 Munger, J. W., Baldocchi, D. D., Liukang, X., Hollinger, D. Y., Richardson, A. D., Stoy, P. C., Siqueira, M. B. S.,  
503 Monson, R. K., Burns, S. P., and Flanagan, L. B.: Evaluation of remote sensing based terrestrial productivity from  
504 MODIS using regional tower eddy flux network observations, *IEEE Transactions on Geoscience and Remote Sensing*,  
505 44, 1908-1925, 10.1109/tgrs.2005.853936, 2006.

506 Huete, A., Didan, K., Miura, T., Rodriguez, E. P., Gao, X., and Ferreira, L. G.: Overview of the radiometric and  
507 biophysical performance of the MODIS vegetation indices, *Remote Sensing of Environment*, 83, 19, 2002.

508 Huete, A. R., Restrepo-Coupe, N., Ratana, P., Didan, K., Saleska, S. R., Ichii, K., Panuthai, S., and Gamo, M.: Multiple  
509 site tower flux and remote sensing comparisons of tropical forest dynamics in Monsoon Asia, *Agricultural and Forest*  
510 *Meteorology*, 148, 748-760, 10.1016/j.agrformet.2008.01.012, 2008.

511 Jiang, Z., Huete, A., Didan, K., and Miura, T.: Development of a two-band enhanced vegetation index without a blue  
512 band, *Remote Sensing of Environment*, 112, 3833-3845, 10.1016/j.rse.2008.06.006, 2008.

513 Joiner, J., Yoshida, Y., Vasilkov, A. P., Yoshida, Y., Corp, L. A., and Middleton, E. M.: First observations of global  
514 and seasonal terrestrial chlorophyll fluorescence from space, *Biogeosciences*, 8, 637-651, 10.5194/bg-8-637-2011,  
515 2011.

516 Julitta, T.: Optical proximal sensing for vegetation monitoring, PhD Dissertation, Department of Earth and  
517 Environmental Sciences, University of Milano-Bicocca, 136 pp., 2015.

518 Jung, M., Reichstein, M., Margolis, H. A., Cescatti, A., Richardson, A. D., Arain, M. A., Arneth, A., Bernhofer, C.,  
519 Bonal, D., Chen, J., Gianelle, D., Gobron, N., Kiely, G., Kutsch, W., Lasslop, G., Law, B. E., Lindroth, A., Merbold,  
520 L., Montagnani, L., Moors, E. J., Papale, D., Sottocornola, M., Vaccari, F., and Williams, C.: Global patterns of land-  
521 atmosphere fluxes of carbon dioxide, latent heat, and sensible heat derived from eddy covariance, satellite, and  
522 meteorological observations, *Journal of Geophysical Research*, 116, 10.1029/2010jg001566, 2011.

523 Köhler, P., Guanter, L., Kobayashi, H., Walther, S., and Yang, W.: Assessing the potential of sun-induced fluorescence  
524 and the canopy scattering coefficient to track large-scale vegetation dynamics in Amazon forests, *Remote Sensing of*  
525 *Environment*, 769-785, 10.1016/j.rse.2017.09.025, 2017.

526 Lasslop, G., Reichstein, M., Detto, M., Richardson, A. D., and Baldocchi, D. D.: Comment on Vickers et al.: Self-  
527 correlation between assimilation and respiration resulting from flux partitioning of eddy-covariance CO<sub>2</sub> fluxes,  
528 *Agricultural and Forest Meteorology*, 150, 312-314, 10.1016/j.agrformet.2009.11.003, 2010.

529 Laurance, W. F., Useche, D. C., Rendeiro, J., Kalka, M., Bradshaw, C. J., Sloan, S. P., Laurance, S. G., Campbell, M.,  
530 Abernethy, K., Alvarez, P., Arroyo-Rodriguez, V., Ashton, P., Benitez-Malvido, J., Blom, A., Bobo, K. S., Cannon,  
531 C. H., Cao, M., Carroll, R., Chapman, C., Coates, R., Cords, M., Danielsen, F., De Dijn, B., Dinerstein, E., Donnelly,  
532 M. A., Edwards, D., Edwards, F., Farwig, N., Fashing, P., Forget, P. M., Foster, M., Gale, G., Harris, D., Harrison,  
533 R., Hart, J., Karpanty, S., Kress, W. J., Krishnaswamy, J., Logsdon, W., Lovett, J., Magnusson, W., Maisels, F.,  
534 Marshall, A. R., McClearn, D., Mudappa, D., Nielsen, M. R., Pearson, R., Pitman, N., van der Ploeg, J., Plumptre, A.,  
535 Poulsen, J., Quesada, M., Rainey, H., Robinson, D., Roetgers, C., Rovero, F., Scatena, F., Schulze, C., Sheil, D.,  
536 Struhsaker, T., Terborgh, J., Thomas, D., Timm, R., Urbina-Cardona, J. N., Vasudevan, K., Wright, S. J., Arias, G. J.,  
537 Arroyo, L., Ashton, M., Auzel, P., Babaasa, D., Babweteera, F., Baker, P., Banki, O., Bass, M., Bila-Isia, I., Blake,  
538 S., Brockelman, W., Brokaw, N., Bruhl, C. A., Bunyavejchewin, S., Chao, J. T., Chave, J., Chellam, R., Clark, C. J.,  
539 Clavijo, J., Congdon, R., Corlett, R., Dattaraja, H. S., Dave, C., Davies, G., Beisiegel Bde, M., da Silva Rde, N., Di  
540 Fiore, A., Diesmos, A., Dirzo, R., Doran-Sheehy, D., Eaton, M., Emmons, L., Estrada, A., Ewango, C., Fedigan, L.,  
541 Feer, F., Fruth, B., Willis, J. G., Goodale, U., Goodman, S., Guix, J. C., Guthiga, P., Haber, W., Hamer, K., Herbinger,  
542 I., Hill, J., Huang, Z., Sun, I. F., Ickes, K., Itoh, A., Ivanauskas, N., Jackes, B., Janovec, J., Janzen, D., Jiangming, M.,  
543 Jin, C., Jones, T., Justiniano, H., Kalko, E., Kasangaki, A., Killeen, T., King, H. B., Klop, E., Knott, C., Kone, I.,  
544 Kudavidanage, E., Ribeiro, J. L., Lattke, J., Laval, R., Lawton, R., Leal, M., Leighton, M., Lentino, M., Leonel, C.,  
545 Lindsell, J., Ling-Ling, L., Linsenmair, K. E., Losos, E., Lugo, A., Lwanga, J., Mack, A. L., Martins, M., McGraw,  
546 W. S., McNab, R., Montag, L., Thompson, J. M., Nabe-Nielsen, J., Nakagawa, M., Nepal, S., Norconk, M., Novotny,  
547 V., O'Donnell, S., Opiang, M., Ouboter, P., Parker, K., Parthasarathy, N., Pisciotta, K., Prawiradilaga, D., Pringle, C.,

548 Rajathurai, S., Reichard, U., Reinartz, G., Renton, K., Reynolds, G., Reynolds, V., Riley, E., Rodel, M. O., Rothman,  
549 J., Round, P., Sakai, S., Sanaiotti, T., Savini, T., Schaab, G., Seidensticker, J., Siaka, A., Silman, M. R., Smith, T. B.,  
550 de Almeida, S. S., Sodhi, N., Stanford, C., Stewart, K., Stokes, E., Stoner, K. E., Sukumar, R., Surbeck, M., Tobler,  
551 M., Tschardtke, T., Turkalo, A., Umapathy, G., van Weerd, M., Rivera, J. V., Venkataraman, M., Venn, L., Vere,  
552 C., de Castilho, C. V., Waltert, M., Wang, B., Watts, D., Weber, W., West, P., Whitacre, D., Whitney, K., Wilkie, D.,  
553 Williams, S., Wright, D. D., Wright, P., Xiankai, L., Yonzon, P., and Zamzani, F.: Averting biodiversity collapse in  
554 tropical forest protected areas, *Nature*, 489, 290-294, 10.1038/nature11318, 2012.

555 Lee, J. E., Frankenberg, C., van der Tol, C., Berry, J. A., Guanter, L., Boyce, C. K., Fisher, J. B., Morrow, E., Worden,  
556 J. R., Asefi, S., Badgley, G., and Saatchi, S.: Forest productivity and water stress in Amazonia: observations from  
557 GOSAT chlorophyll fluorescence, *Proceedings. Biological sciences / The Royal Society*, 280, 20130171,  
558 10.1098/rspb.2013.0171, 2013.

559 Lewis, S. L., Lloyd, J., Sitch, S., Mitchard, E. T. A., and Laurance, W. F.: Changing Ecology of Tropical Forests:  
560 Evidence and Drivers, *Annual Review of Ecology, Evolution, and Systematics*, 40, 529-549,  
561 10.1146/annurev.ecolsys.39.110707.173345, 2009.

562 Liangyun Liu, X. L., ZhihuiWang, and Bing Zhang: Measurement and Analysis of BidirectionalSIF Emissions in  
563 Wheat Canopies, *IEEE TRANSACTIONS ON GEOSCIENCE AND REMOTE SENSING*, 12, 2016.

564 Liu, J., Bowman, K. W., Schimel, D. S., Parazoo, N. C., Jiang, Z., Lee, M., Bloom, A. A., Wunch, D., Frankenberg,  
565 C., Sun, Y., O'Dell, C. W., Gurney, K. R., Menemenlis, D., Gierach, M., Crisp, D., and Eldering, A.: Contrasting  
566 carbon cycle responses of the tropical continents to the 2015-2016 El Nino, *Science*, 358, eaam5690,  
567 10.1126/science.aam5690, 2017.

568 Liu, L., Yang, X., Gong, F., Su, Y., Huang, G., and Chen, X.: The Novel Microwave Temperature Vegetation Drought  
569 Index (MTVDI) Captures Canopy Seasonality across Amazonian Tropical Evergreen Forests, *Remote Sensing*, 13,  
570 10.3390/rs13030339, 2021.

571 Liu, X., Liu, L., Zhang, S., and Zhou, X.: New Spectral Fitting Method for Full-Spectrum Solar-Induced Chlorophyll  
572 Fluorescence Retrieval Based on Principal Components Analysis, *Remote Sensing*, 7, 10626-10645,  
573 10.3390/rs70810626, 2015.

574 Logan, B. A., Adams, W. W., and Demmig-Adams, B.: Viewpoint:Avoiding common pitfalls of chlorophyll  
575 fluorescence analysis under field conditions, *Functional Plant Biology*, 34, 853, 10.1071/fp07113, 2007.

576 Magney, T. S., Frankenberg, C., Fisher, J. B., Sun, Y., North, G. B., Davis, T. S., Kornfeld, A., and Siebke, K.:  
577 Connecting active to passive fluorescence with photosynthesis: a method for evaluating remote sensing measurements  
578 of Chl fluorescence, *The New phytologist*, 1594-1608, 10.1111/nph.14662, 2017.

579 Malenovsky, Z., Mishra, K. B., Zemek, F., Rascher, U., and Nedbal, L.: Scientific and technical challenges in remote  
580 sensing of plant canopy reflectance and fluorescence, *Journal of experimental botany*, 60, 2987-3004,  
581 10.1093/jxb/erp156, 2009.

582 Malhi, Y.: The productivity, metabolism and carbon cycle of tropical forest vegetation, *Journal of Ecology*, 100, 65-  
583 75, 10.1111/j.1365-2745.2011.01916.x, 2012.

584 Medlyn, B. E.: Physiological basis of the light use efficiency model, *Tree Physiology*, 18, 167-176,  
585 <https://doi.org/10.1093/treephys/18.3.167>, 1998.

586 Meroni, M., Rossini, M., Guanter, L., Alonso, L., Rascher, U., Colombo, R., and Moreno, J.: Remote sensing of solar-  
587 induced chlorophyll fluorescence: Review of methods and applications, *Remote Sensing of Environment*, 113, 2037-  
588 2051, 10.1016/j.rse.2009.05.003, 2009.

589 Merrick, Pau, Jorge, Bennartz, and Silva: Spatiotemporal Patterns and Phenology of Tropical Vegetation Solar-  
590 Induced Chlorophyll Fluorescence across Brazilian Biomes Using Satellite Observations, *Remote Sensing*, 11,  
591 10.3390/rs11151746, 2019.

592 Merrick, T., Jorge, M. L. S. P., Silva, T. S. F., Pau, S., Rausch, J., Broadbent, E. N., and Bennartz, R.: Characterization  
593 of chlorophyll fluorescence, absorbed photosynthetically active radiation, and reflectance-based vegetation index  
594 spectroradiometer measurements, *International Journal of Remote Sensing*, 41, 6755-6782,  
595 10.1080/01431161.2020.1750731, 2020.

596 Mitchard, E. T. A.: The tropical forest carbon cycle and climate change, *Nature*, 559, 527-534, 10.1038/s41586-018-  
597 0300-2, 2018.

598 Monteith, J.L., Climate and the efficiency of crop production in Britain, *Phil. Trans. R. Soc. Land.*, 281, 277-294,  
599 1977.

600 Morton, D. C., Rubio, J., Cook, B. D., Gastellu-Etchegorry, J. P., Longo, M., Choi, H., Hunter, M. O., and Keller, M.:  
601 Amazon forest structure generates diurnal and seasonal variability in light utilization, *Biogeosciences Discussions*,  
602 12, 19043-19072, 10.5194/bgd-12-19043-2015, 2015.

603 Morton, D. C., Nagol, J., Carabajal, C. C., Rosette, J., Palace, M., Cook, B. D., Vermote, E. F., Harding, D. J., and  
604 North, P. R.: Amazon forests maintain consistent canopy structure and greenness during the dry season, *Nature*, 506,  
605 221-224, 10.1038/nature13006, 2014.

606 Moya, I., Camenen, L., Evain, S., Goulas, Y., Cerovic, Z. G., Latouche, G., Flexas, J., and Ounis, A.: A new instrument  
607 for passive remote sensing1. Measurements of sunlight-induced chlorophyll fluorescence, *Remote Sensing of  
608 Environment*, 91, 186-197, 10.1016/j.rse.2004.02.012, 2004.

609 Plascyk, J. A.: The MK II Fraunhofer Line Discriminator (FLD -II) for Airborne and Orbital Remote Sensing of Solar-  
610 Stimulated Luminescence, *Optical Engineering*, 14, 8, 1975.

611 Porcar-Castell, A., Tyystjarvi, E., Atherton, J., van der Tol, C., Flexas, J., Pfundel, E. E., Moreno, J., Frankenberg, C.,  
612 and Berry, J. A.: Linking chlorophyll a fluorescence to photosynthesis for remote sensing applications: mechanisms  
613 and challenges, *Journal of experimental botany*, 65, 4065-4095, 10.1093/jxb/eru191, 2014.

614 R Development Core Team: R: A language and environment for statistical computing, R Foundation for Statistical  
615 Computing [code], 2010.

616 Rocha, A. V., Appel, R., Bret-Harte, M. S., Euskirchen, E. S., Salmon, V., and Shaver, G.: Solar position confounds  
617 the relationship between ecosystem function and vegetation indices derived from solar and photosynthetically active  
618 radiation fluxes, *Agricultural and Forest Meteorology*, 298-299, 10.1016/j.agrformet.2020.108291, 2021.

619 Rong Li, F. Z.: Accuracy assessment on reconstruction algorithms of solar-induced Fluorescence Spectrum,  
620 *Geoscience and Remote Sensing Symposium (IGARSS) IEEE International*, 1727-1730,

621 Rossini, M., Alonso, L., Cogliati, S., Damm, A., Guanter, L., Julitta, T., Meroni, M., Moreno, J., Panigada, C., Pinto,  
622 F., Rascher, U., Schickling, A., Schüttemeyer, D., Zemek, F., and Colombo, R.: Measuring sun-induced chlorophyll  
623 fluorescence: An evaluation and synthesis of existing field data, 5th International workshop on remote sensing of  
624 vegetation fluorescence, Paris, France, 1-5,

625 Rouse Jr, J. W., Haas, R. H., Schell, J. A., and Deering, D. W.: Paper A 20, hird Earth Resources Technology Satellite-  
626 1 Symposium: The Proceedings of a Symposium Goddard Space Flight Center at Washington, DC 309,

627 Running, S. W., Nemani, R. R., Heinsch, F. A., Zhao, M., Reeves, M., and Hashimoto, H.: A Continuous Satellite-  
628 Derived Measure of Global Terrestrial Primary Production, *BioScience*, 54, 547-551, 2004.

629 Ryu, Y., Jiang, C., Kobayashi, H., and Detto, M.: MODIS-derived global land products of shortwave radiation and  
630 diffuse and total photosynthetically active radiation at 5 km resolution from 2000, *Remote Sensing of Environment*,  
631 204, 812-825, 10.1016/j.rse.2017.09.021, 2018.

632 Saatchi, S. S., Harris, N. L., Brown, S., Lefsky, M., A., E. T., Mitchare, W. S., Zutta, B. R., Buerman, W., Lewis, S.  
633 L., Hagen, S., Petrova, S., White, L., Silman, M., and Morel, A.: Benchmark map of forest carbon stocks in tropical  
634 regions across three continents, *Proceedings of the National Academy of Sciences*, 108, 9899-9905, 2010.

635 Saatchi, S. S., Harris, N. L., Brown, S., Lefsky, M., Mitchard, E. T., Salas, W., Zutta, B. R., Buermann, W., Lewis, S.  
636 L., Hagen, S., Petrova, S., White, L., Silman, M., and Morel, A.: Benchmark map of forest carbon stocks in tropical  
637 regions across three continents, *Proceedings of the National Academy of Sciences of the United States of America*,  
638 108, 9899-9904, 10.1073/pnas.1019576108, 2011.

639 Samanta, A., Ganguly, S., and Myneni, R.: MODIS Enhanced Vegetation Index data do not show greening of Amazon  
640 forests during the 2005 drought, *New Phytologist*, 189, 4, 2010.

641 Schickling, A., Matveeva, M., Damm, A., Schween, J., Wahner, A., Graf, A., Crewell, S., and Rascher, U.: Combining  
642 Sun-Induced Chlorophyll Fluorescence and Photochemical Reflectance Index Improves Diurnal Modeling of Gross  
643 Primary Productivity, *Remote Sensing*, 8, 574, 10.3390/rs8070574, 2016.

644 Sims, D., Rahman, A., Cordova, V., Elmasri, B., Baldocchi, D., Bolstad, P., Flanagan, L., Goldstein, A., Hollinger,  
645 D., and Misson, L.: A new model of gross primary productivity for North American ecosystems based solely on the  
646 enhanced vegetation index and land surface temperature from MODIS, *Remote Sensing of Environment*, 112, 1633-  
647 1646, 10.1016/j.rse.2007.08.004, 2008.

648 Springer, K., Wang, R., and Gamon, J. A.: Parallel Seasonal Patterns of Photosynthesis, Fluorescence, and Reflectance  
649 Indices in Boreal Trees, *Remote Sensing*, 9, 1-18, 10.3390/rs9070691, 2017.

650 Sun, Y., Frankenberg, C., Wood, J. D., Schimel, D. S., Jung, M., Guanter, L., Drewry, D. T., Verma, M., Porcar-  
651 Castell, A., Griffis, T. J., Gu, L., Magney, T. S., Kohler, P., Evans, B., and Yuen, K.: OCO-2 advances photosynthesis  
652 observation from space via solar-induced chlorophyll fluorescence, *Science*, 358, eaam5747,  
653 10.1126/science.aam5747, 2017.

654 Torrence, C. and Compo, G. P.: A Practical Guide to Wavelet Analysis, *Bulletin of the American Meteorological  
655 Society*, 79, 61-79, 1998.

656 Tucker, C., Red and photographic infrared linear combinations for vegetation monitoring, *Remote Sensing of  
657 Environment*, 8, 127-150,1979.

658 Turner, D. P., Ritts, W. D., Cohen, W. B., Gower, S. T., Zhao, M., Running, S. W., Wofsy, S. C., Urbanski, S., Dunn,  
659 A. L., and Munger, J. W.: Scaling Gross Primary Production (GPP) over boreal and deciduous forest landscapes in  
660 support of MODIS GPP product validation, *Remote Sensing of Environment*, 88, 256-270, 10.1016/j.rse.2003.06.005,  
661 2003.

662 Van Wittenberghe, S., Alonso, L., Verrelst, J., Moreno, J., and Samson, R.: Bidirectional sun-induced chlorophyll  
663 fluorescence emission is influenced by leaf structure and light scattering properties — A bottom-up approach, *Remote*  
664 *Sensing of Environment*, 158, 169-179, 10.1016/j.rse.2014.11.012, 2015.

665 Van Wittenberghe, S., Alonso, L., Verrelst, J., Hermans, I., Delegido, J., Veroustraete, F., Valcke, R., Moreno, J., and  
666 Samson, R.: Upward and downward solar-induced chlorophyll fluorescence yield indices of four tree species as  
667 indicators of traffic pollution in Valencia, *Environmental pollution*, 173, 29-37, 10.1016/j.envpol.2012.10.003, 2013.

668 Wang, C., Beringer, J., Hutley, L. B., Cleverly, J., Li, J., Liu, Q., and Sun, Y.: Phenology Dynamics of Dryland  
669 Ecosystems Along the North Australian Tropical Transect Revealed by Satellite Solar-Induced Chlorophyll  
670 Fluorescence, *Geophysical Research Letters*, 46, 5294-5302, 10.1029/2019gl082716, 2019.

671 Wang, S., Zhang, Y., Ju, W., Qiu, B., and Zhang, Z.: Tracking the seasonal and inter-annual variations of global gross  
672 primary production during last four decades using satellite near-infrared reflectance data, *The Science of the total*  
673 *environment*, 755, 142569, 10.1016/j.scitotenv.2020.142569, 2020.

674 Wickham, H.: *ggplot2: Elegant Graphics for Data Analysis*, Springer-Verlag [code], 2016.

675 Wickham, H.: *tidyverse: Easily Install and Load the 'Tidyverse' (R package*  
676 *version 1.2.1) [code]*, 2017.

677 Wickham, H., François, R., Henry, L., and Müller, K.: *dplyr: A Grammar of Data Manipulation (R package version*  
678 *0.7.8) [code]*, 2018.

679 Wright, S. J.: The future of tropical forests, *Ann N Y Acad Sci*, 1195, 1-27, 10.1111/j.1749-6632.2010.05455.x, 2010.

680 Wu, G., Guan, K., Jiang, C., Peng, B., Kimm, H., Chen, M., Yang, X., Wang, S., Suyker, A. E., Bernacchi, C. J.,  
681 Moore, C. E., Zeng, Y., Berry, J. A., and Cendrero-Mateo, M. P.: Radiance-based NIRv as a proxy for GPP of corn  
682 and soybean, *Environmental Research Letters*, 15, 10.1088/1748-9326/ab65cc, 2020.

683 Xu, L., Saatchi, S. S., Yang, Y., Myneni, R. B., Frankenberg, C., Chowdhury, D., and Bi, J.: Satellite observation of  
684 tropical forest seasonality: spatial patterns of carbon exchange in Amazonia, *Environmental Research Letters*, 10,  
685 084005, 10.1088/1748-9326/10/8/084005, 2015.

686 Yang, H., Yang, X., Zhang, Y., Heskell, M. A., Lu, X., Munger, J. W., Sun, S., and Tang, J.: Chlorophyll fluorescence  
687 tracks seasonal variations of photosynthesis from leaf to canopy in a temperate forest, *Glob Chang Biol*, 23, 2874-  
688 2886, 10.1111/gcb.13590, 2017.

689 Yang, J., Tian, H., Pan, S., Chen, G., Zhang, B., and Dangal, S.: Amazon droughts and forest responses: Largely  
690 reduced forest photosynthesis but slightly increased canopy greenness during the extreme drought of 2015/2016, *Glob*  
691 *Chang Biol*, 1919-1934, 10.1111/gcb.14056, 2018a.

692 Yang, K., Ryu, Y., Dechant, B., Berry, J. A., Hwang, Y., Jiang, C., Kang, M., Kim, J., Kimm, H., Kornfeld, A., and  
693 Yang, X.: Sun-induced chlorophyll fluorescence is more strongly related to absorbed light than to photosynthesis at  
694 half-hourly resolution in a rice paddy, *Remote Sensing of Environment*, 216, 658-673, 10.1016/j.rse.2018.07.008,  
695 2018b.

696 Yang, P., van der Tol, C., Campbell, P. K. E., and Middleton, E. M.: Fluorescence Correction Vegetation Index  
697 (FCVI): A physically based reflectance index to separate physiological and non-physiological information in far-red  
698 sun-induced chlorophyll fluorescence, *Remote Sensing of Environment*, 240, 10.1016/j.rse.2020.111676, 2020.

699 Yuan, W., Cai, W., Xia, J., Chen, J., Liu, S., Dong, W., Merbold, L., Law, B., Arain, A., Beringer, J., Bernhofer, C.,  
700 Black, A., Blanken, P. D., Cescatti, A., Chen, Y., Francois, L., Gianelle, D., Janssens, I. A., Jung, M., Kato, T., Kiely,  
701 G., Liu, D., Marcolla, B., Montagnani, L., Raschi, A., Rouspard, O., Varlagin, A., and Wohlfahrt, G.: Global  
702 comparison of light use efficiency models for simulating terrestrial vegetation gross primary production based on the  
703 LaThuile database, *Agricultural and Forest Meteorology*, 192–193, 108–120,  
704 <https://doi.org/10.1016/j.agrformet.2014.03.007>, 2014.

705 Zarco-Tejada, P. J., González-Dugo, V., and Berni, J. A. J.: Fluorescence, temperature and narrow-band indices  
706 acquired from a UAV platform for water stress detection using a micro-hyperspectral imager and a thermal camera,  
707 *Remote Sensing of Environment*, 117, 322-337, 10.1016/j.rse.2011.10.007, 2012.

708 Zarco-Tejada, P. J., Morales, A., Testi, L., and Villalobos, F. J.: Spatio-temporal patterns of chlorophyll fluorescence  
709 and physiological and structural indices acquired from hyperspectral imagery as compared with carbon fluxes  
710 measured with eddy covariance, *Remote Sensing of Environment*, 133, 102-115, 10.1016/j.rse.2013.02.003, 2013.

711 Zarco-Tejada, P. J., Miller, J. R., Mohammed, G. H., Noland, T. L., and Sampson, P. H.: Estimation of chlorophyll  
712 fluorescence under natural illumination from hyperspectral data, *International Journal of Applied Earth Observation*  
713 *and Geoinformation*, 3, 7, 2001.

714 Zeng, Y., Badgley, G., Dechant, B., Ryu, Y., Chen, M., and Berry, J. A.: A practical approach for estimating the  
715 escape ratio of near-infrared solar-induced chlorophyll fluorescence, *Remote Sensing of Environment*, 232,  
716 10.1016/j.rse.2019.05.028, 2019.

717 Zhang, Z., Zhang, Y., Zhang, Q., Chen, J. M., Porcar-Castell, A., Guanter, L., Wu, Y., Zhang, X., Wang, H., Ding,  
718 D., and Li, Z.: Assessing bi-directional effects on the diurnal cycle of measured solar-induced chlorophyll fluorescence  
719 in crop canopies, *Agricultural and Forest Meteorology*, 295, 10.1016/j.agrformet.2020.108147, 2020.

720 Zhang, Z., Zhang, Y., Zhang, Y., Gobron, N., Frankenberg, C., Wang, S., and Li, Z.: The potential of satellite FPAR  
721 product for GPP estimation: An indirect evaluation using solar-induced chlorophyll fluorescence, *Remote Sensing of*  
722 *Environment*, 240, 10.1016/j.rse.2020.111686, 2020.

723 Zhao, M., Running, S., Heinsch, F. A., and Nemani, R.: MODIS-Derived Terrestrial Primary Production, 11, 635-  
724 660, 10.1007/978-1-4419-6749-7\_28, 2010.

725 Zhu, X. and Liu, D.: Improving forest aboveground biomass estimation using seasonal Landsat NDVI time-series,  
726 *ISPRS Journal of Photogrammetry and Remote Sensing*, 102, 222-231, 10.1016/j.isprsjprs.2014.08.014, 2015.

727

728